Hindawi Publishing Corporation
Journal of Robotics
Volume 2015, Article ID 791865, 13 pages
http://dx.doi.org/10.1155/2015/791865

Research Article

Development and Motion Testing of a Robotic Ray

Jianhui He and Yonghua Zhang

Department of Mechatronics Engineering, Taizhou Vocational & Technical College, Taizhou 318000, China

Correspondence should be addressed to Jianhui He; hjh1103@mail.ustc.edu.cn

Received 16 October 2014; Revised 26 December 2014; Accepted 9 January 2015

Academic Editor: Nan Xiao

Biomimetics takes nature as a model for inspiration to immensely help abstract new principles and ideas to develop various devices for real applications. In order to improve the stability and maneuvering of biomimetic fish like underwater propulsors, we selected bluespotted ray that propel themselves by taking advantage of their pectoral fins as target. First, a biomimetic robotic undulating fin driven propulsor was built based on the simplified pectoral structure of living bluespotted ray. The mechanical structure and control circuit were then presented. The fin undulating motion patterns, fin ray angle, and fin shape to be investigated are briefly introduced. Later, the kinematic analysis of fin ray and the whole fin is discussed. The influence of various kinematic parameters and morphological parameters on the average propulsion velocity of the propulsor was analyzed. Finally, we conclude that the average propulsion velocity generally increases with the increase of kinematic parameters such as frequency, amplitude, and wavelength, respectively. Moreover, it also has a certain relationship with fin undulating motion patterns, fin ray angle, fin shape, and fin aspect ratio.

1. Introduction

Each fish species has its own unique way of interacting with different environments, which then dictates the species' shape and size, as well as the way it propels itself, through a process of natural selection. Therefore, fish provide useful illustrations of propulsor design, swimming modes, and body/fin shape (morphology). An estimated 15% of the fish families in the word use median and pectoral fins, termed median and/or paired fin (MPF) locomotion [1]. Obviously, batoids are very famous for their MPF locomotion who exhibit two modes of pectoral swimming behavior: (1) undulatory locomotion, termed "rajiform" and (2) oscillatory locomotion, termed "mobuliform." Rajiform locomotion is performed by skates and most stingrays and involves undulatory waves that are propagated down the fins from anterior to posterior [2, 3]. Compared with body and/or caudal fin (BCF) locomotion fishes, batoids have remarkable manoeuvrability and can efficiently stabilize themselves in currents and surges and are more hydromechanically efficient at low-speeds than BCF periodic swimmers [4]. They leave a less noticeable wake than BCF locomotion fishes and are capable of turning on their own axis with little or no lateral translation of the body [5–7]. These characteristics make batoid fishes an ideal platform to emulate in the design of a bioinspired autonomous underwater vehicle (AUV).

On the other hand, the demands for general aquatic locomotion research, environmental protection, ocean exploration, military reconnaissance, data gathering, search and rescue devices, video exploration, and remote maintenance operations have become more urgent and desirable than ever before. But the high cost of performing such operations with ship based platforms prevents researchers from probing the oceans extensively [8]. Thus, with the development of low-cost robotic technologies, several teams have developed the robotics prototype resembling real fish with MPF modes. Figure 1 illustrates some relevant robotic fishes developed and tested [1, 9–36]. The biomimetic undulating fin mechanisms were developed by using various actuators, such as motor [9–30], parallel bellows actuator (PBA) [1], IPMC [31–34], and SMA [35, 36].

An important design consideration for swimming machines is the design of propulsors: their shape, location on the machine, pattern of movement, and mechanical and material properties (e.g., inertia and stiffness). The overall shape of the robot is another important consideration. As

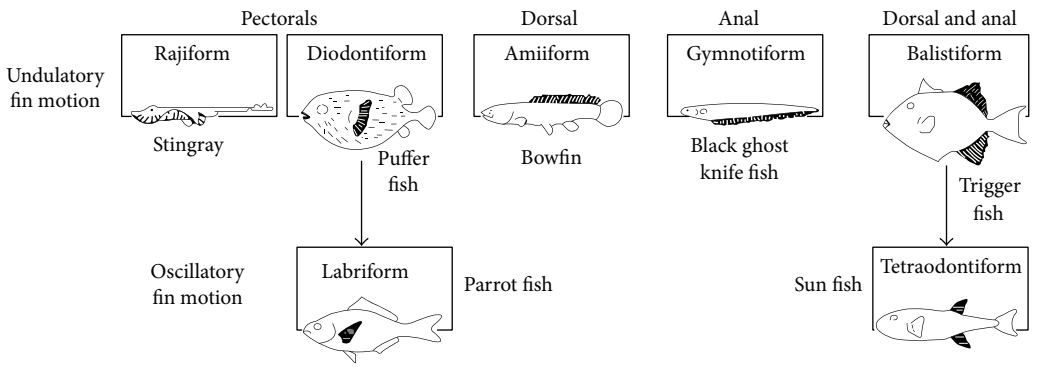

(a)

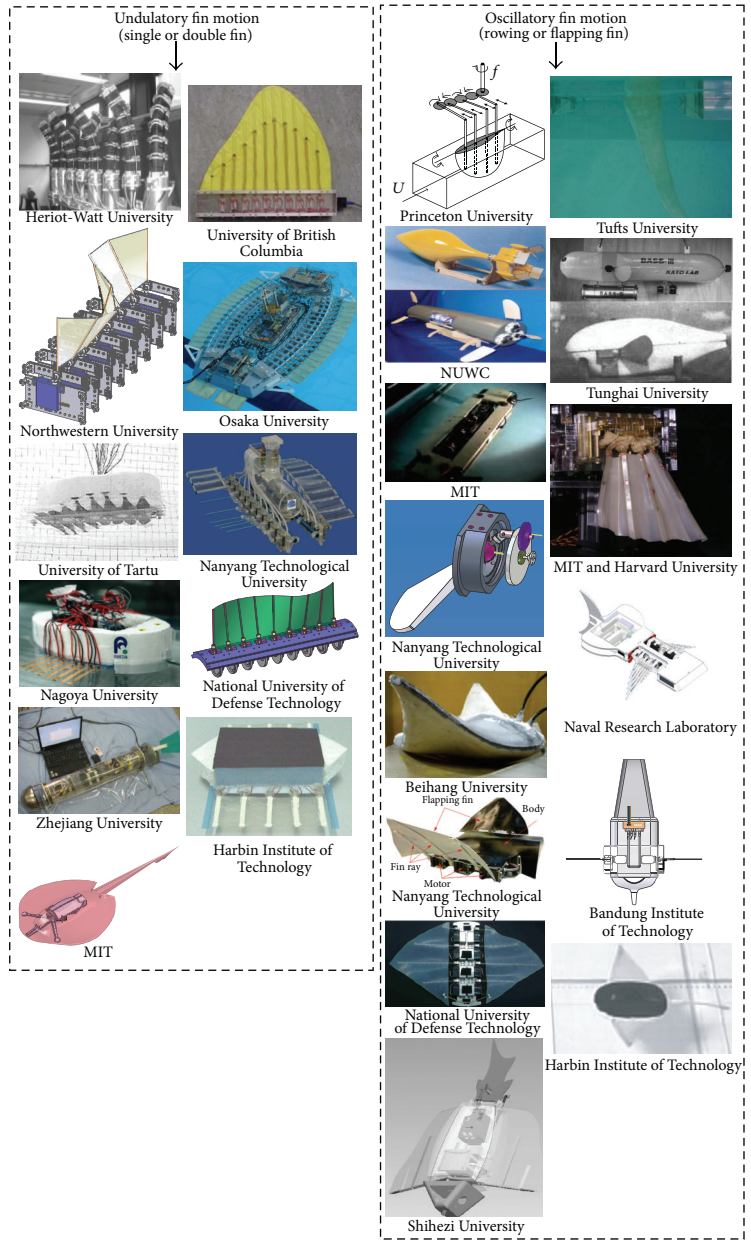

(b)

Figure 1: Swimming modes of fishes using MPF propulsion. Hatched areas in Figure 2(a) shows the propulsive segment that contributes to thrust generation. Figure 2(b) shows the robotic fishes that use MPF modes [1, 9–36].

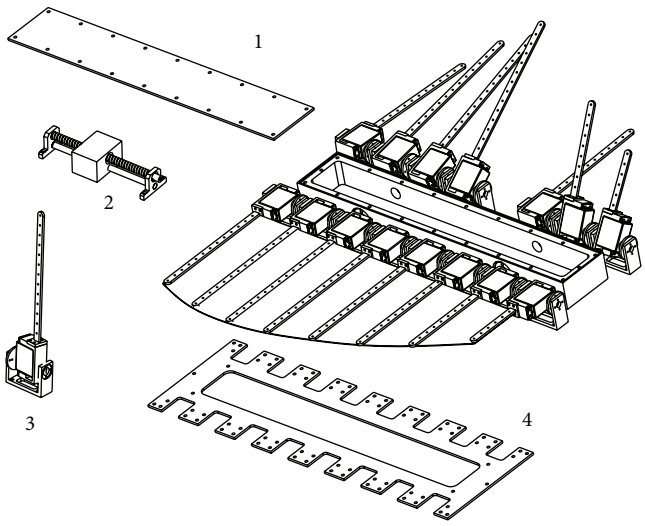

(a)

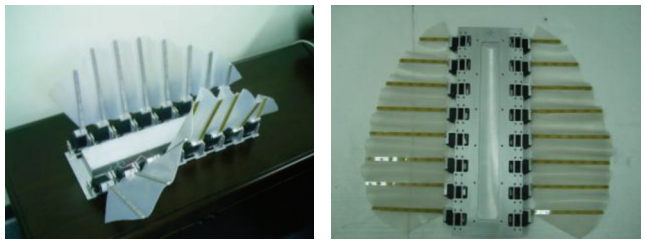

(b)

Figure 2: Layout of prototype. 1. Lid; 2. center of gravity adjustment mechanism; 3. oscillating module; 4. baseboard.

fish are impressive swimmers in many ways, it is hoped that submersible robots that swim like fish might be superior to submersibles using propellers [37]. Our long term goal is to develop an AUV that is capable of civil or military application. However, PBA actuators are too clumsy and require complex gas supply system. SMA actuators are highly nonlinear and possibly difficult to achieve precise deformation control. Meanwhile, the output power of IPMC actuators is too small. Thus, from the perspective of practical application, motor actuators may be not optical but much feasible.

Several motor driven robotic undulating fins based AUVs have already been built. Despite the fact that all of these robots aim to provide alternatives to propellers, their propulsion mechanisms differ substantially. Accordingly, we subdivide it into three types: (1) a mechanical implementation relying on camshafts to generate the propagating wave which comes at the price of limited flexibility of parameter variation [18]. (2) the oscillating motion of fin rays is independently controlled by servomotors, and alternate oscillation of fin rays can produce undulating motion on fin membrane [16, 17]. (3) The undulating motion of the whole robotic fin is produced by oscillating motion of a single anteriorly equipped fin ray, and the vibration subsequently spreads to the rear end [12]. The abovementioned second type could be categorized into two types depending on the way the fin rays are connected. One is the fin rays that are parallel-arranged and connected on a fixed baseline [16, 17]. The other one is the fin rays that are connected on a free baseline through cranks. Each crank is directly driven by a motor and baseline moves as all cranks oscillate [11]. Unlike the prototype built by BOILEAU [16], we simplify the oscillating mechanism and make the whole structure much more compact and reliable.

The present work is concerned with the design of bluespotted ray inspired underwater propulsor possessing two large lateral expanded undulating fins and the parametric study of propulsion performance. The rest of paper is organized as follows. In Section 2, we present detailed mechanism design. The undulating patterns, fin ray angle, and fin shape to be investigated are also briefly introduced. In Section 3, kinematic analysis of the proposed mechanism is proposed. In Section 4, the influence of various kinematic parameters and morphological parameters on the average propulsion velocity of the propulsor was analyzed. Finally, the work is concluded with some remarks.

2. Mechanism and Control

Kier and Thompson suggested that the fins of a stingray are supported by three dimensional arrays of muscle [38]. Existing actuators, both linear and rotary, are unable to model the complex musculature of these fins. Despite the complexity of the actual musculature, the fins of a stingray exhibit much the same undulations as those displayed by the fins of ray-finned fish using an undulatory swimming mode. As a possible simplification, the fin of a stingray is divided into many segments such that the fin looks similar to that of a ray-finned fish.

2.1. Mechanical Structure. Figure 2 shows the mechanical structure of bluespotted ray like biorobotic underwater propulsor with a modular undulating fin consisting of eight equally spaced servomotors attached to a lightweight structure on both sides. The prototype design of the developed robot comprises three individual modules: two pectoral fin modules, electronics housing module, and center of gravity adjustment module. Tail is not considered for simplicity. The propulsor is an exact copy of the bluespotted ray anatomy, with a length of 0.71 m and width of 0.64 m, which fully mimics the anatomical dimensions of a mature ray.

Thereinto, the fin ray element consists of shaft sleeve, fixed nut, steering-gear bracket, steering-gear seat, and steering gear, shown in Figure 3. The housing is used to install battery, control electronics, and center of gravity adjustment module. All of them are installed on the baseboard. The prototype owns built-in energy sources. It is a self-sufficient prototype and gives an autonomy of 30 minutes of operation at moderate velocities. Meanwhile, two batteries provide the electrical energy required by electronics and control system components. The total batteries capacity is 3200 mAh. The mechanical design of the actuator system and the other sections provide robotic ray with the maximum interior capacity compared to the overall volume. This feature enables further modifications and makes the system suitable for additional accessory placements. The microcontroller (Altera

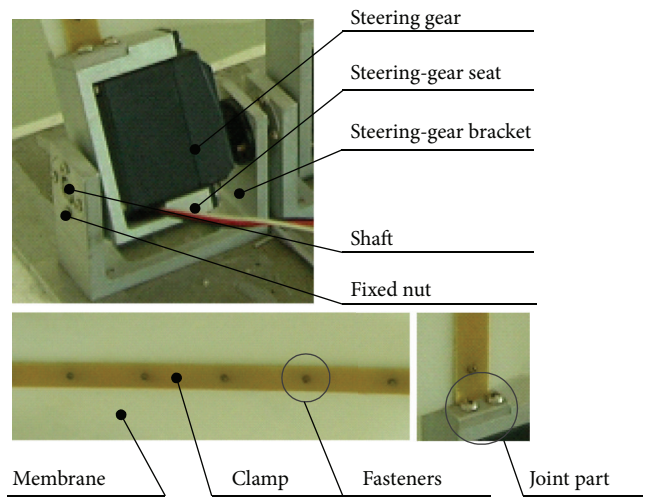

Figure 3: Oscillating module structure.

Table 1: Parameters of robotic ray.

Parameter	Unit	Values of robotic ray	Values of real bluespotted ray [3]
Total length	mm	710	710
Total width	mm	640	640
Total height	mm	42	42
The weight of the entire robot	kg	4.7	—
Fin ray number	—	8	>200
Fin ray length	mm	Adjustable	10~220
Fin ray width	mm	10	0.3~1.0
Fin ray height	mm	3	0.3~1.0
Fin ray space	mm	64.5 (equal distance)	<2.0 (nonequidistance)
Fin ray obliquity	°	30~90 (adjustable)	−100~85
Surface width	mm	462.5	710
Membrane modulus of elasticity	MPa	2.7	0.14
Frequency	Hz	≤3	≤3
Amplitude	°	≤60	≤45
Wavelength	mm	>475	355~890
Drive mode	—	Motor	Muscle

Max II, CPLD) based built-in control system controls the fin motions. Backed up with optical sensors which are used for environment exploration, this stand-alone system is the first step to the full autonomy of the prototype. Fin rays are made of elastic material (polypropylene) in order to add compliance of motion. This design is simpler than those using smart materials [39, 40] or multijoint linkage mechanisms [41–43]. Fin rays are designed as uniform strength cantilever beams in order to reduce the mass without causing structure failure in oscillations. Fin membrane is made of silicon rubber. The physical specifications of robotic ray are listed in Table 1.

2.2. Control. The fin of the real fish consists of fin rays that have varying span and stiffness with a flexible membrane connecting them together. Analogously, we develop a modular robotic fin which enables us to experiment with different materials for the rays and flexible membrane, each fin ray is directly connected to its corresponding driver motor. The advantages of this direct-connection mode are that the amplitude, frequency, and phase of each fin ray can be independently controlled. Each motor drives a radial insert, the angle of which could be changed from 30° to 90° from the robotic ray centerline. The motor up/down moves the radial inserts generating waves that propagate along the circumference of the body. The control electronics provide a pulse width modulated (PWM) signal to control the amplitude and frequency of rotation of each motor. The motors operate at a standard voltage of 4.8 volts. At these volts, each motor delivers 8.0 kg·cm of torque and rotates at a maximum speed equivalent to 0.10 sec/60°. STR-36 series micropower wireless module is used as the wireless data transceiver in short-ranges. The outward appearance and modules of the control electronics board are shown in Figure 4.

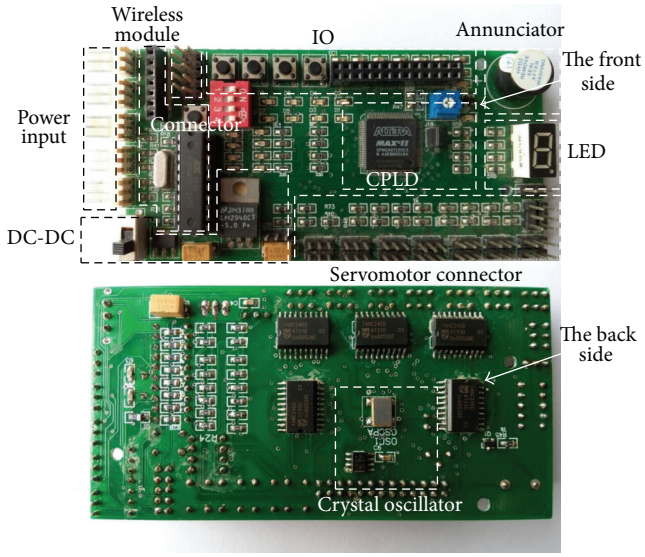

Figure 4: The control electronics.

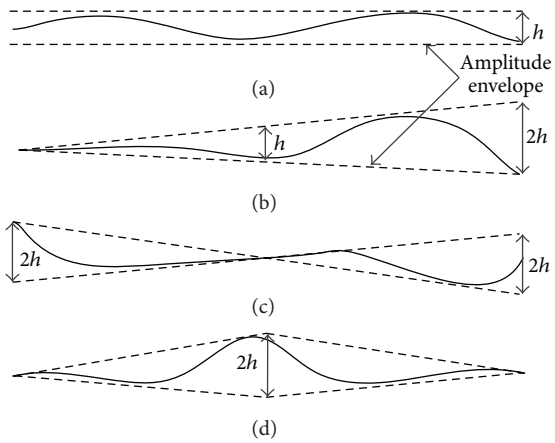

Figure 5: Four typical amplitude envelopes of modular undulating fin. (a) The amplitude envelope is fairly constant along the fins (Mode 1). (b) The amplitude envelope gradually increased from the anterior part to the posterior (Mode 2). (c) The amplitude envelope decreases from the anterior part to the mid part and increases toward the posterior (Mode 3). (d) The amplitude envelope increases from the anterior part to the mid part and decreases toward the posterior (Mode 4).

2.3. Undulating Patterns of the Robotic Ray. Some qualitative observations predicted that the propulsion velocity produced by the robotic ray is different among various fin undulating patterns. To reveal the regularity of this initial finding, four typical undulating fin patterns are selected and compared, with the same amplitude envelope area as well as some other kinematic parameters, such as frequency, wavelength, and wave propulsion velocity (Figure 5).

2.4. Fin Shape of Robotic Ray. In order to investigate the influence of fin morphology on propulsion performance, three morphologies of fins (triangle, rectangle, and trapezoid) are performed with the same undulating patterns and surface area (Table 2).

Table 2: List of three morphologies of fins.

Name	Fin shape	Aspect ratio	Fin area
Rectangle		0.8	
Trapezoid		1	0.45 m^2
Triangle		0.8, 1.0, 1.2, 1.4, 1.6	

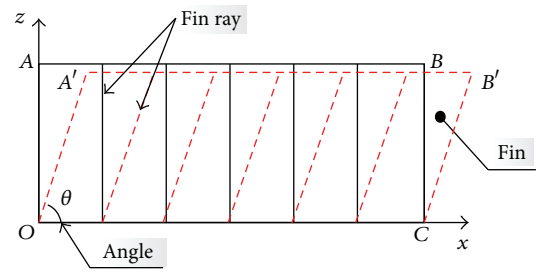

(a) Constant fin ray length

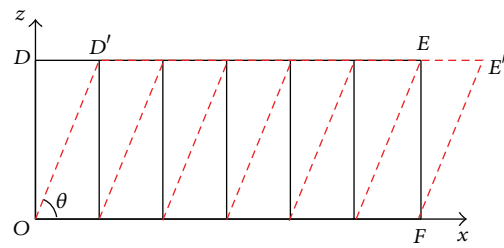

(b) Constant fin area

Figure 6: Two cases of the change of fin ray angle (a) constant fin ray length and (b) constant fin area.

2.5. Fin Ray Angle of Robotic Ray. The influence of fin ray angle on propulsion velocity is another consideration in our experimental investigation. Two cases are tested here. One is that the fin ray length keeps constant when its angle changes and thus the fin surface accordingly varies (Figure 6(a)). The other case is that the fin ray length varies when its angle changes to keep the fin surface constant (Figure 6(b)).

3. Modeling

3.1. Definition of Coordinate System. Figure 7 shows the definition of reference coordinate system. There are four main coordinate systems: earth coordinate system $O_wX_wY_wZ_w$, body coordinate system $o_tx_ty_tz_t$, fin coordinate system $o_q^{I(II)}x_q^{I(II)}y_q^{I(II)}z_q^{I(II)}$, and fin ray coordinate system $o_r^{I(II)}x_r^{I(II)}y_r^{I(II)}z_r^{I(II)}$. Thereinto, body coordinate system is used for swimming kinematics description, meanwhile reflecting the motion state of biology relative to earth coordinate

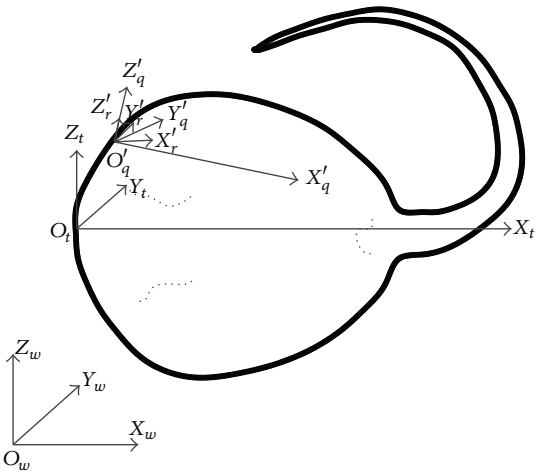

Figure 7: Definition of reference coordinate system.

system; fin coordinate system describes the undulatory movement characteristics of pectoral fins while fin ray coordinate system describes the up/down movement characteristics of fin rays.

The relationship among these coordinate systems is as follows.

(1) The relationship between fin coordinate system and fin ray coordinate system is given by

$$\begin{pmatrix} x_q \\ y_q \\ z_q \end{pmatrix} = \begin{bmatrix} \sin\alpha & \cos\alpha & 0 \\ -\cos\alpha & \sin\alpha & 0 \\ 0 & 0 & 1 \end{bmatrix} \begin{pmatrix} x_r \\ y_r \\ z_r \end{pmatrix} + \begin{pmatrix} x_{r0} \\ y_{r0} \\ z_{r0} \end{pmatrix}, \quad (1)$$

where α is the angle between fin ray and fin baseline. In our prototype, $\alpha = \pi/2$. $[x_{r0}\ \ y_{r0}\ \ z_{r0}]$ means the origin coordinates translation.

(2) The relationship between fin coordinate system and body coordinate system is given by

$$\begin{pmatrix} x_t \\ y_t \\ z_t \end{pmatrix} = \begin{bmatrix} \cos\beta & \sin\beta & 0 \\ -\sin\beta & \cos\beta & 0 \\ 0 & 0 & 1 \end{bmatrix} \begin{pmatrix} x_q \\ y_q \\ z_q \end{pmatrix} + \begin{pmatrix} X_{qo} \\ Y_{qo} \\ Z_{qo} \end{pmatrix}, \quad (2)$$

where β is the angle between fin baseline and body centerline. In our prototype, $\beta = 0$.

(3) The relationship between body coordinate system and earth coordinate system is given by

$$\begin{pmatrix} x' \\ y' \\ z' \end{pmatrix} = \begin{bmatrix} \cos\theta\cos\varphi & \sin\varphi\cos\theta & -\sin\theta \\ -\cos\gamma\sin\varphi + \sin\gamma\sin\theta\cos\varphi & \cos\varphi\cos\gamma + \sin\gamma\sin\theta\sin\varphi & \sin\gamma\cos\theta \\ \sin\gamma\sin\varphi + \cos\gamma\sin\theta\cos\varphi & \cos\gamma\sin\theta\sin\varphi - \sin\gamma\cos\varphi & \cos\gamma\cos\theta \end{bmatrix} \begin{pmatrix} x \\ y \\ z \end{pmatrix} + \begin{pmatrix} x_{t0} \\ y_{t0} \\ z_{t0} \end{pmatrix}, \quad (3)$$

where θ, φ, and γ are the rotation angles around the three axes.

3.2. Kinematic Analysis on Fin Ray. Similar to Shirgaonkar et al. [13], Epstein et al. [17], and Hu et al. [18], undulating fin can be modeled as a ruled surface in 3D space. The fin baseline is the directrix of the ruled surface, while the fin ray is the generatrix. The undulation can then be generated through a sequential up/down motion of generatrix on the ruled surface. If we assume that all the fin rays' up/down motion are under the same sinusoidal waveforms. In the fin ray coordinate system, the space coordinate of a point $P(x_r, y_r, z_r)$ on the ith fin ray can be described as follows:

$$\begin{aligned} x_r &= 0, \\ y_r &= L_{ip}\cos\left(\theta_{fi}(i,t)\right), \\ z_r &= L_{ip}\sin\left(\theta_{fi}(i,t)\right), \end{aligned} \quad (4)$$

where L_{ip} is the distance from point P to fin ray base; $\theta_{fi}(i,t)$ is the angular position of the ith fin ray at time t given by

$$\theta_{fi}(i,t) = \theta_{fi\max}(x_i)\sin\left(\frac{2\pi t}{T_i} - \theta_{0i}\right), \quad (5)$$

where

$$\begin{aligned} \theta_{fi\max}(x_i) &= \arcsin\left(\frac{f(x_i)}{L_{ir}}\right), \\ f(x_i) &= f(x)\big|_{x=x_i}, \\ \theta_{0i} &= 2\pi\frac{(i-1)}{N}\frac{L}{\lambda}. \end{aligned} \quad (6)$$

$\theta_{fi\max}(x_i)$ is the amplitude of the wave at the ith fin ray; T_i is the up/down motion cycle, $T_i = T$; θ_{0i} is the initial phase of the ith fin ray; L_{ir} is the length of the ith fin ray; N is the total number of rays; λ is the wavelength; and L is the fin length. Thus, (4) can be rewritten as

$$\begin{aligned} x_r &= 0, \\ y_r &= L_{ip}\cos\left(\arcsin\left(\frac{f(x_i)}{L_{ir}}\right)\sin\left(\frac{2\pi t}{T_i} - 2\pi\frac{(i-1)}{N}\frac{L}{\lambda}\right)\right), \\ z_r &= L_{ip}\sin\left(\arcsin\left(\frac{f(x_i)}{L_{ir}}\right)\sin\left(\frac{2\pi t}{T_i} - 2\pi\frac{(i-1)}{N}\frac{L}{\lambda}\right)\right). \end{aligned} \quad (7)$$

Observation of ray swimming strongly suggests that the amplitude along the fin ray is not linear. The assumption of

a linear variation along the fin ray in this study is to simplify the analysis. We further get fin ray up/down motion angular velocity and angular acceleration through the first derivation and the second derivation of (5):

$$\omega_{fi}(i,t) = \frac{d\theta_{fi}(i,t)}{dt} = \frac{2\pi\theta_{fi\max}}{T}\cos\left(\frac{2\pi t}{T} - \theta_{0i}\right),$$
$$a_{fi}(i,t) = \frac{d^2\theta_{fi}(i,t)}{dt^2} = -\frac{4\pi^2\theta_{fi\max}}{T^2}\sin\left(\frac{2\pi t}{T} - \theta_{0i}\right). \quad (8)$$

As indicated in (8), at the maximum up/down motion angle, the fin ray angular velocity is zero, while the acceleration reaches its maximum and vice versa.

3.3. Kinematic Analysis on Undulatory Fin. For present study, we idealize fin kinematics as a travelling sinusoid on an otherwise stationary (i.e., nontranslating and nonrotating) membrane. As a consequence, the baseline of the fin remains fixed at all times, and all points on the fin from baseline to distal edge move in a sinusoidal manner.

In the fin coordinate system (Figure 8), the coordinate of a point $S(x_q, y_q, z_q)$ on fin surface can be described as follows:

$$\begin{bmatrix} x_q \\ y_q \\ z_q \end{bmatrix} = \mathbf{I}\begin{bmatrix} 0 \\ L_s\cos(\theta_f) \\ L_s\sin(\theta_f) \end{bmatrix} + \begin{bmatrix} o_qo_r \\ 0 \\ 0 \end{bmatrix}. \quad (9)$$

$\begin{bmatrix} 0 \\ L_s\cos(\theta_f) \\ L_s\sin(\theta_f) \end{bmatrix}$ is the coordinate of point S in the fin ray coordinate system. $\begin{bmatrix} o_qo_r \\ 0 \\ 0 \end{bmatrix}$ is the translation matrix, where

$$\theta_f = \theta_{f\max}(x_q)\sin\left[2\pi\left(\frac{t}{T} - \frac{x_q}{\lambda}\right)\right],$$
$$\theta_{f\max}(x_q) = \arcsin\left(\frac{f(x_q)}{L_{rq}}\right). \quad (10)$$

$\mathbf{I}$ is the rotary matrix; in this case, it is an identity matrix. L_s is the distance from point S to baseline. θ_f is the angle between O_rS and y_r axis. $f(x_q)$ is value of amplitude envelope function at x_q. Equation (11) is further expressed as

$$\begin{bmatrix} x_q \\ y_q \\ z_q \end{bmatrix} = \begin{bmatrix} x_q \\ L_s\cos\left(\arcsin\left(\frac{f(x_q)}{L_{rq}}\right)\sin\left[2\pi\left(\frac{t}{T} - \frac{x_q}{\lambda}\right)\right]\right) \\ L_s\sin\left(\arcsin\left(\frac{f(x_q)}{L_{rq}}\right)\sin\left[2\pi\left(\frac{t}{T} - \frac{x_q}{\lambda}\right)\right]\right) \end{bmatrix}. \quad (11)$$

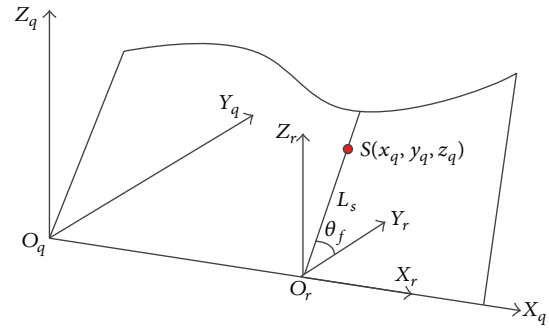

Figure 8: Kinematics modeling of undulatory fin.

The kinematics equation of biomimetic fin is then expressed as follows:

$$y_q(x_q, z_q, t) = A(x_q, z_q)\sin(\omega t - kx_q), \quad (12)$$

where $\omega = 2\pi f$ is undulatory angular frequency, $k = 2\pi/\lambda$ is wave number, and $A(x_q, z_q)$ is amplitude.

Here, if the fin ray is not perpendicular to fin base. That is, the angle between fin ray and x_q axis is θ ($\theta \neq \pi/2$); a more general form of (13) could be expressed below:

$$y_q(x_q, z_q, \theta, t) = \frac{z_q\sqrt{1 + c\tan^2(\theta)}}{\gamma}\sin\left[\omega t - 2\pi\left(\frac{x_q - z_q c\tan(\theta)}{\lambda}\right)\right], \quad (13)$$

where γ is the fin ray slope.

From (13), we notice that the kinematics equation of biomimetic fin is relative to kinematic parameters such as frequency (f), amplitude (A), wavelength (λ), and morphological parameters such as the angle between fin ray and x_q axis (θ). By adjusting them, various locomotion patterns produced by real ray could also be achieved by biorobotic underwater propulsor. The kinematics analysis conducted above helps a lot in the following experiments investigation.

3.4. Propulsion Velocity Analysis of Robotic Ray. According to (13), we use the law of conservation of momentum to integrate water quality that is enveloped by the undulating fin.

If we consider $\theta = \pi/2$, at the beginning ($t \approx 0$), (13) can be simplified to

$$y_q(x_q, z_q, 0) = A(x_q, z_q)\sin(kx_q). \quad (14)$$

It is reasonable to ignore the bending deformation of fin rays during motion since their material is aluminium alloy. We safely assume that the fin amplitude is linear change. Thus the fluid mass between ΔABC and $\Delta A'B'C'$ (Figure 9) is expressed as

$$dM_{\text{water}}\frac{1}{2}|y_q|\sqrt{Lr^2 - {y_q}^2}dx_q, \quad (15)$$

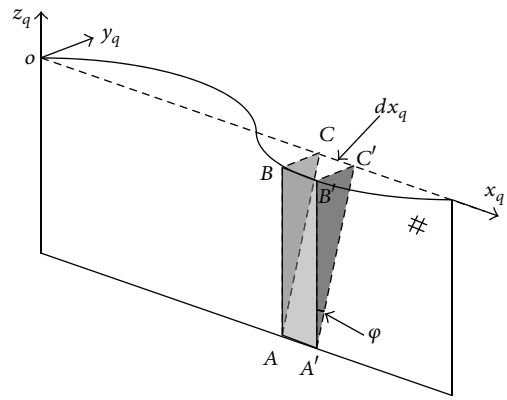

Figure 9: Propulsion velocity analysis of robotic ray.

where Lr is fin ray length, and the total fluid mass is calculated as below:

$$M_{\text{water}} = \frac{1}{2}\rho_{\text{water}} \int_0^{\tau\lambda} \left|y_q\right| \sqrt{Lr^2 - {y_q}^2}\, dx_q, \tag{16}$$

where ρ_{water} is density of fluid (e.g., water) and τ is natural number. Consider one full wavelength ($\tau = 1$), add (14) to (16), and then

$$\begin{aligned} M_{\text{water}} &= \frac{1}{2}\rho_{\text{water}} \int_0^{\lambda} \left|A\sin\left(kx_q\right)\right| \sqrt{Lr^2 - A^2\sin^2\left(kx_q\right)}\, dx_q \\ &= \rho_{\text{water}} \int_0^{\lambda/2} A\sin\left(kx_q\right) \sqrt{Lr^2 - A^2\sin^2\left(kx_q\right)}\, dx_q. \end{aligned} \tag{17}$$

From Figure 9 we have $\sqrt{Lr^2 - A^2\sin^2(kx_q)} = Lr\cos(\varphi)$; then

$$M_{\text{water}} = \frac{2\rho_{\text{water}} ALr\cos\left(\varphi\right)}{k} \sin^2\left(\frac{\lambda k}{4}\right). \tag{18}$$

On the other hand, we have the following relations:

$$\mathbf{V} = \mathbf{V}_{\text{water}} + \mathbf{V}_{\text{fin}}. \tag{19}$$

Here $\mathbf{V}$ represents the velocity of fluid (pushed by fin surface) relative to fin; $\mathbf{V}_{\text{water}}$ represents the velocity of fluid relative to earth coordinate system; $\mathbf{V}_{\text{fin}}$ represents the velocity of fin relative to earth coordinate system. At the beginning, $\mathbf{V} \approx 0$, so the fluid drag on the fin surface can be ignored, using the law of conservation of momentum:

$$M_{\text{water}} \times \mathbf{V}_{\text{water}} = M_{\text{fin}} \times \mathbf{V}_{\text{fin}}. \tag{20}$$

Thus

$$\mathbf{V}_{\text{fin}} = \mathbf{V} - \mathbf{V}_{\text{water}} = \frac{M_{\text{water}}}{M_{\text{water}} + M_{\text{fin}}}\mathbf{V}, \tag{21}$$

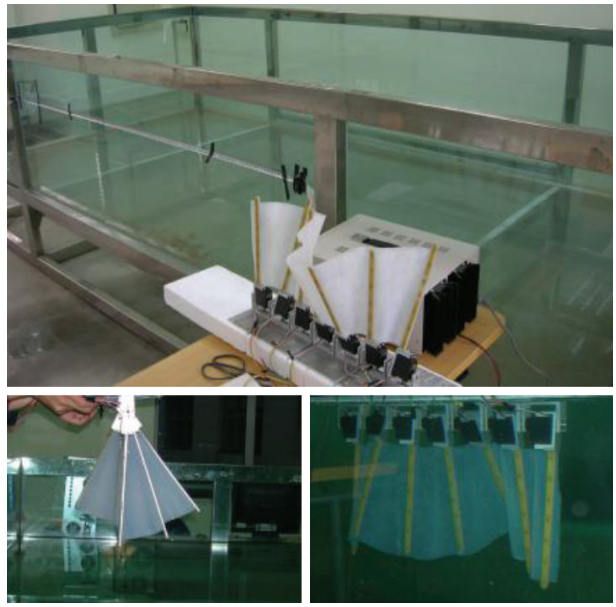

Figure 10: Water tank for free swimming test.

where $\mathbf{V} = \lambda f = \omega\lambda/2\pi$, and we finally have

$$\begin{aligned} \mathbf{V}_{\text{fin}} &= \frac{\left(2\rho_{\text{water}} ALr\cos\left(\varphi\right)/k\right)\sin^2\left(\lambda k/4\right)}{\left(2\rho_{\text{water}} ALr\cos\left(\varphi\right)/k\right)\sin^2\left(\lambda k/4\right) + M_{\text{fin}}} \left(\frac{\omega\lambda}{2\pi}\right) \\ &= \zeta\left(\frac{\omega\lambda}{2\pi}\right), \end{aligned} \tag{22}$$

where

$$\zeta = \frac{\left(2\rho_{\text{water}} ALr\cos\left(\varphi\right)/k\right)\sin^2\left(\lambda k/4\right)}{\left(2\rho_{\text{water}} ALr\cos\left(\varphi\right)/k\right)\sin^2\left(\lambda k/4\right) + M_{\text{fin}}}, \quad (0 < \zeta < 1) \tag{23}$$

where ζ means the influence of geometrical characteristic and amplitude on the propulsion velocity of robotic ray. Theoretically speaking, we conclude that $\mathbf{V}_{\text{fin}}$ is directly proportional to ω and λ. What is more, $\mathbf{V}_{\text{fin}}$ is in a certain proportion to A, Lr, and ρ_{water} and increases with them.

4. Experiments

The experimental systems for both free swimming and restricted forward straight swimming test of robotic fin are depicted below.

4.1. Experimental System for Free Swimming Test. Experimental system for free swimming test is shown in Figure 10. A high-speed video system (out of sight) (SpeedCAM) operates at 100 images per second with maximum resolution ratio of 512 × 512 pixels. The camera was placed above the flow tank to capture images in dorsal view. Images were obtained by the multichannel monochrome image acquisition card. Then, a computer operating system with human-computer interaction interface processed and analyzed images.

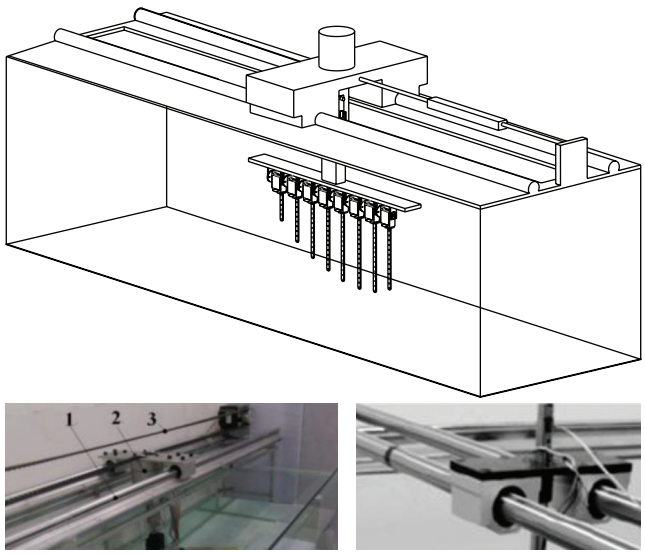

Figure 11: Experimental system for restricted forward straight swimming test. 1. Linear motion guide. 2. Fin clamp bracket. 3. Velocity sensor.

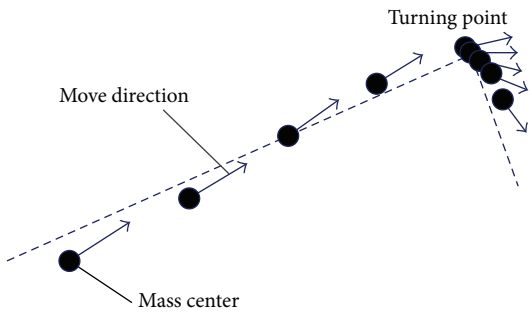

Figure 12: Trajectory tracking.

4.2. Experimental System for Restricted Forward Straight Swimming Test. Figure 11 is the experimental system for restricted forward straight swimming test. Most of current tests are conducted using this experimental system, such as the tests to investigate the influence of kinematic parameters and morphological parameters on averaged propulsion velocity. It consists of linear motion guide, fin clamp bracket, and velocity sensor. The robotic fin is fixed to the clamp bracket which can move along linear motion guide due to the undulating motion of robotic fin, and its motion velocity is detected and recorded by velocity sensor.

5. Results

5.1. Free Swimming Test. A single undulating fin was adopted to conduct the free swimming test in the water tank, including forward/backward and turning motion. By taking advantage of high speed camera, we tracked the motion trajectory of fin shown in Figure 12. The black spot represents mass center of fin, and the arrows mean its moving direction. When symmetrically oscillate fin ray, the fin surface receives symmetrical force from surrounding fluid and thus achieves straight moving. The turning motion of a single fin could be realized by bias-oscillating of fin ray.

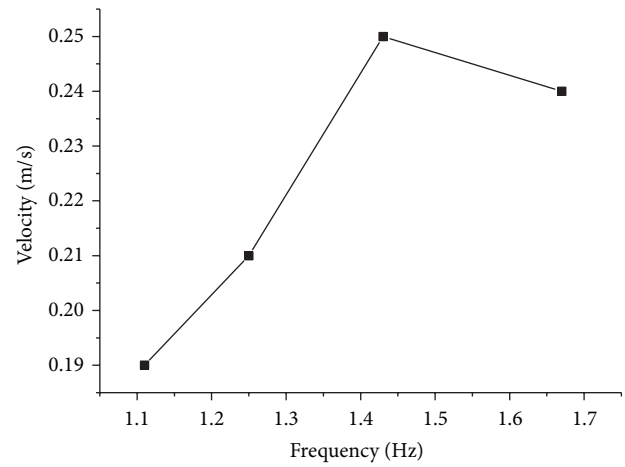

Figure 13: Relationship between averaged propulsion velocity and frequency.

5.2. Influence of Kinematic Parameters on Propulsion Velocity. We adopt four different frequencies (1.11 Hz, 1.25 Hz, 1.43 Hz, and 1.67 Hz), amplitudes (60 mm, 80 mm, 100 mm, and 120 mm) and wavelengths (256 mm, 322.5 mm, 387 mm, and 451.5 mm). The control variables method is used here and the results are shown below.

Figure 13 shows the relationship between averaged propulsion velocity and frequency. The increase of averaged propulsion velocity is almost directly proportional to that of frequency, which is consistent with the above theoretical calculation results. However, when frequency reaches a certain value (around 1.45 Hz in our test), the velocity decreases with the increase of frequency. The main reason may be that a higher frequency of the robotic ray may cause a more drastic disturbance to the surrounding fluid. Due to the limitation of experimental conditions, the disturbance cannot be fully extended and disappeared in the experimental tank. Furthermore, the reflected wave from the tank wall may further interfere with the performance of robotic ray, which causes the decrease of its velocity.

Figure 14 shows the relationship between averaged propulsion velocity and amplitudes. Similarly, the increase of averaged propulsion velocity is almost directly proportional to that of amplitudes, which is also consistent with the above theoretical calculation results.

Figure 15 shows the relationship between averaged propulsion velocity and wavelengths. At the beginning, the averaged propulsion velocity increases with the increase of wavelength, which is also consistent with the above theoretical calculation results. But a longer wavelength may flatten undulating curve. Due to the fluid viscosity, the velocity of fluid enveloped by the fin cannot reach the wave propagate velocity. Therefore, when wavelength reaches

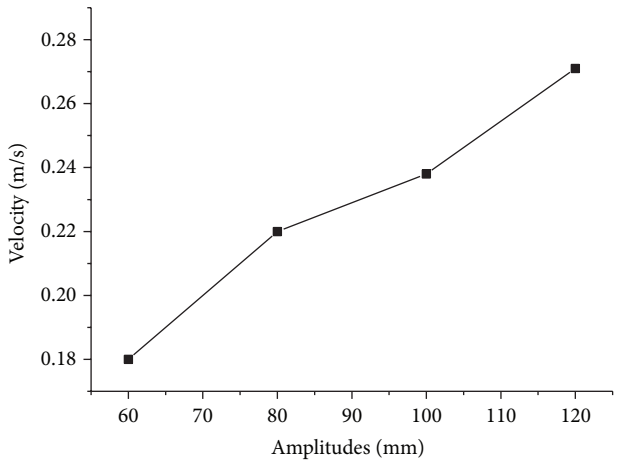

Figure 14: Relationship between averaged propulsion velocity and amplitudes.

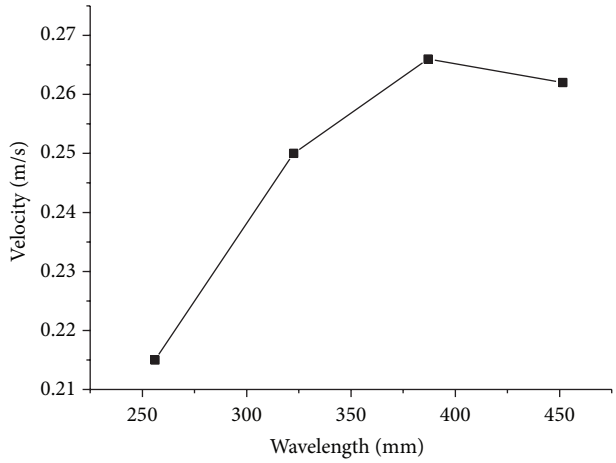

Figure 15: Relationship between averaged propulsion velocity and wavelengths.

a certain value (around 387 mm in our test), the velocity decreases with the further increase of wavelength.

5.3. Influence of Fin Undulating Patterns on Propulsion Velocity. Figure 16 shows the influence of different undulating patterns on averaged propulsion velocity of robotic fin. It is observed from Figure 16 that the amplitude envelope increases from the anterior part to the mid part and decreases toward the posterior (similar to real ray fin motion pattern) produceing the highest velocity than the other three patterns. The averaged propulsion velocity of Mode 4 is about 0.271 m/s, while for Mode 1, Mode 2, and Mode 3 it is about 0.248 m/s, 0.238 m/s, and 0.182 m/s, respectively. Therefore, the fin in Mode 3 swims most slowly. It is also very interesting to highlight that seldom fishes in nature adopt this mode to propel themselves.

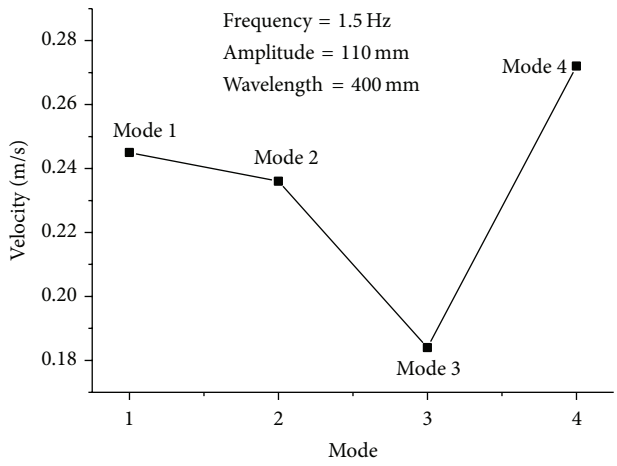

Figure 16: Influence of different undulating modes on averaged propulsion velocity. (a) The amplitude envelope is fairly constant along the fins (Mode 1). (b) The amplitude envelope gradually increased from the anterior part to the posterior (Mode 2). (c) The amplitude envelope decreases from the anterior part to the mid part and increases toward the posterior (Mode 3). (d) The amplitude envelope increases from the anterior part to the mid part and decreases toward the posterior (Mode 4).

5.4. Influence of Morphology Parameters on Propulsion Velocity

5.4.1. Fin Ray Angle. Three morphology parameters are considered: fin ray angle, fin shape, and fin aspect ratio. Figure 17 shows relationship between averaged propulsion velocity and fin ray angle. In the case of constant fin ray length (Figure 6(a)), the propulsion velocity increases with the increase of fin ray angle. It is not difficult to understand why it happens. When the fin ray angle increased, the fin surface area is growing accordingly in this case, the propulsion thrust may be subsequently increased which results in acceleration of propulsion velocity. In the case of constant fin area (Figure 6(b)), the propulsion velocity decreases with the increase of angle of fin ray; however, the tendency is reduced. The reason of which still confuses us and remains to be further investigated.

5.4.2. Fin Shape. Figure 18 is the relationship between averaged propulsion velocity and fin shape. As mentioned before, three typical fin shapes are discussed here: rectangle, triangle, and trapezoid. We find that the triangular fin is able to produce the highest propulsion velocity at 0.266 m/s. This fin morphology is observed in numerous batoid fishes.

5.4.3. Fin Aspect Ratio. We further select triangular fin to investigate influence of its aspect ratio on propulsion velocity at the same kinematic parameters. The aspect ratio is defined as the ratio of stretched length to chord length. Five values (0.8, 1.0, 1.2, 1.4, and 1.6) are easily achieved by change the robotic fin ray length as well as their spacing. The results are illustrated in Figure 19. With the increase of aspect ratio, the propulsion velocity is observably increased. We wonder

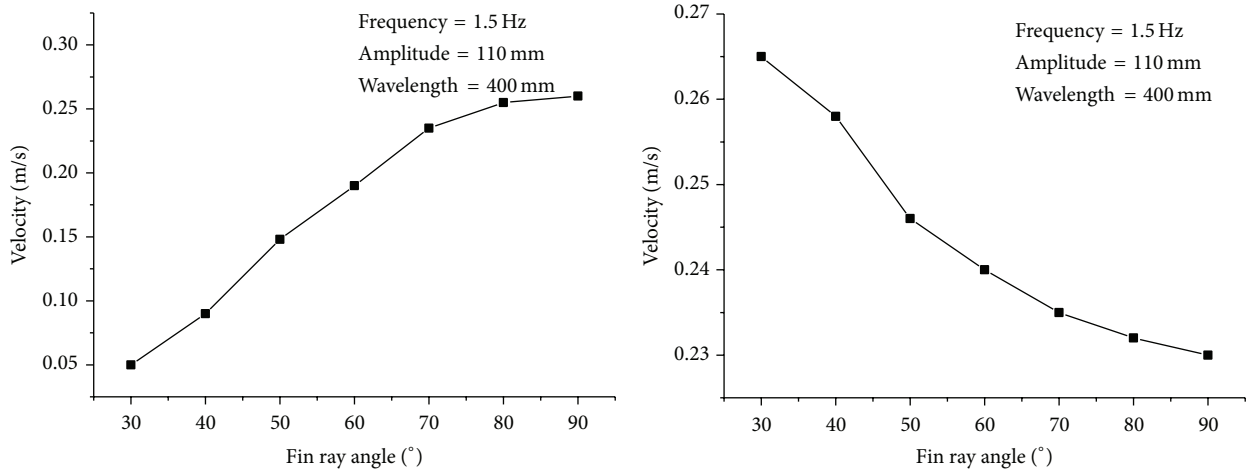

(a) Constant fin ray length

(b) Constant fin area

Figure 17: Relationship between averaged propulsion velocity and fin ray angle.

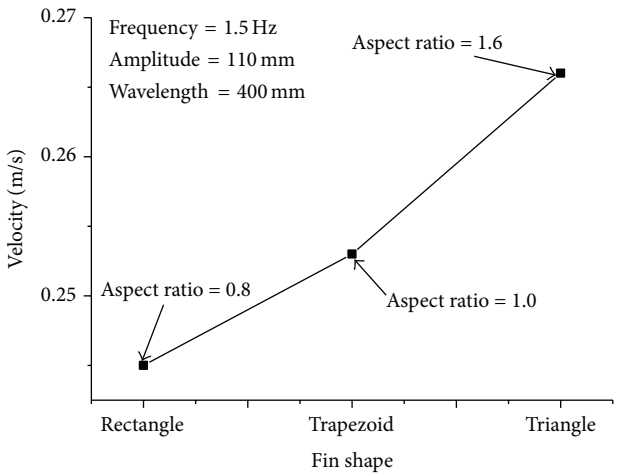

Figure 18: Relationship between averaged propulsion velocity and fin shape.

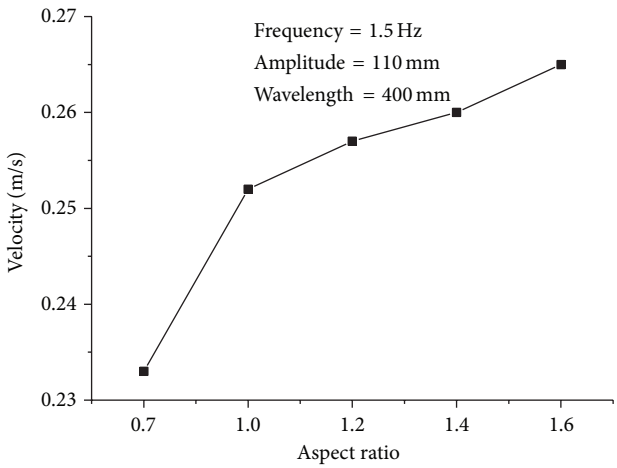

Figure 19: Relationship between averaged propulsion velocity and fin aspect ratio.

whether the change of propulsion velocity among different fin shapes may relate to the difference in aspect ratio.

6. Conclusions

In this paper, a robotic ray has been built based on the simplified pectoral structure of living bluespotted ray. The mechanical structure and control circuit are presented. Kinematic analysis on the fin ray and the full fin is discussed. The influence of various kinematic parameters and morphology parameters on the propulsion velocity of the robotic ray is analyzed using both theoretical and experimental methods. We finally conclude the following.

(1) The averaged propulsion velocity of robotic ray is almost directly proportional to increase of frequency, amplitude, and wavelength.

(2) The averaged propulsion velocity of robotic ray has a certain relationship with its morphological parameters such as fin shape. Meanwhile, in the case of constant fin ray length, the propulsion velocity increases with the increase of fin ray angle. In the case of constant fin area, the propulsion velocity decreases with the increase of angle of fin ray. As for the aspect ratio, the propulsion velocity is observably increased with the increase of it.

(3) The amplitude envelope increases from the anterior part to the mid part and decreases toward the posterior (similar to real ray fin motion pattern) producing the highest velocity than the other three patterns. Combining with the fin shape, we may make a bold statement that the undulating pattern has a certain relationship with fin shape.

Our future work will focus on design, implement, and test control strategies involving two fins. Additionally, to analyze the efficiency and compare it quantitatively (a) with other undulation robots and (b) with other methods of propulsion

such as propellers is considered. Finally, the reason why the propulsion velocity decreases with the increase of angle of fin ray at the constant fin area remains to be further discussed. The relationship between motion pattern and fin shape will also be investigated later.

Conflict of Interests

The authors declare that there is no conflict of interests regarding the publication of this paper.

Acknowledgment

The authors would first like to thank Professor JIA Laibing of University of Science and Technology of China for his support on the works over these years. The funds (2014YB01) and (2015YB02) supported by TZVTC (Taizhou Vocational and Technical College) are also acknowledged.

References

[1] M. Sfakiotakis, D. M. Lane, and B. C. Davies, "An experimental undulating-fin device using the Parallel Bellows Actuator," in *Proceedings of the IEEE International Conference on Robotics and Automation*, pp. 2356–2362, Seoul, Republic of Korea, May 2001.

[2] L. J. Rosenberger and M. W. Westneat, "Functional morphology of undulatory pectoral fin locomotion in the stingray *Taeniura Lymma* (Chondrichthyes: Dasyatidae)," *The Journal of Experimental Biology*, vol. 202, no. 24, pp. 3523–3539, 1999.

[3] L. J. Rosenberger, "Pectoral fin locomotion in batoid fishes: undulation *versus* oscillation," *The Journal of Experimental Biology*, vol. 204, no. 2, pp. 379–394, 2001.

[4] M. Listak, G. Martin, D. Pugal, A. Aabloo, and M. Kruusmaa, "Design of a semiautonomous biomimetic underwater vehicle for environmental monitoring," in *Proceedings of the IEEE International Symposium on Computational Intelligence in Robotics and Automation (CIRA '05)*, pp. 9–14, Espoo, Finland, June 2005.

[5] R. W. Blake, "On seahorse locomotion," *Journal of the Marine Biological Association of the United Kingdom*, vol. 56, no. 4, pp. 939–949, 1976.

[6] R. W. Blake, "On ostraciiform locomotion," *Journal of the Marine Biological Association of the United Kingdom*, vol. 57, no. 4, pp. 1047–1055, 1977.

[7] R. W. Blake, "On balistiform locomotion," *Journal of the Marine Biological Association of the United Kingdom*, vol. 58, no. 1, pp. 73–80, 1978.

[8] 2013, http://www.qing-yun.com.

[9] E. Blevins and G. V. Lauder, "Swimming near the substrate: a simple robotic model of stingray locomotion," *Bioinspiration and Biomimetics*, vol. 8, no. 1, Article ID 016005, 2013.

[10] P. E. Sitorus, Y. Y. Nazaruddin, E. Leksono, and A. Budiyono, "Design and implementation of paired pectoral fins locomotion of *Labriform* fish applied to a fish robot," *Journal of Bionic Engineering*, vol. 6, no. 1, pp. 37–45, 2009.

[11] K. H. Low and A. Willy, "Biomimetic motion planning of an undulating robotic fish fin," *Journal of Vibration and Control*, vol. 12, no. 12, pp. 1337–1359, 2006.

[12] P. V. Alvarado, S. Chin, W. Larson, A. Mazumdar, and K. Youcef-Toumi, "A soft body under-actuated approach to multi degree of freedom biomimetic robots: a stingray example," in *Proceedings of the 3rd IEEE RAS and EMBS International Conference on Biomedical Robotics and Biomechatronics*, pp. 473–478, Tokyo, Japan, September 2010.

[13] A. A. Shirgaonkar, O. M. Curet, N. A. Patankarm, and M. A. MacIver, "The hydrodynamics of ribbon-fin propulsion during impulsive motion," *The Journal of Experimental Biology*, vol. 211, no. 21, pp. 3490–3503, 2008.

[14] F. Liu, C. Yang, Q. Su, D. Wang, and Y. Zhang, "Simulation analysis and experimental research on the movements of biomimetic fin," *Journal of Mechanical Engineering*, vol. 46, no. 19, pp. 24–29, 2010.

[15] P. R. Bandyopadhyay, "Trends in biorobotic autonomous undersea vehicles," *IEEE Journal of Oceanic Engineering*, vol. 30, no. 1, pp. 109–139, 2005.

[16] R. Boileau, L. Fan, and T. Moore, *Mechanization of Rajiform Swimming Motion: The Making of Robo-Ray*, University of British Columbia, 2002.

[17] M. Epstein, J. E. Colgate, and M. A. MacIver, "A biologically inspired robotic ribbon fin," in *Proceedings of the IEEE/RSJ International Conference on Intelligent Robots and Systems, Workshop on Morphology, Control, and Passive Dynamics*, pp. 2412–2417, Edmonton, Canada, 2005.

[18] T. Hu, L. Shen, L. Lin, and H. Xu, "Biological inspirations, kinematics modeling, mechanism design and experiments on an undulating robotic fin inspired by *Gymnarchus niloticus*," *Mechanism and Machine Theory*, vol. 44, no. 3, pp. 633–645, 2009.

[19] R. P. Clark and A. J. Smits, "Thrust production and wake structure of a batoid-inspired oscillating fin," *Journal of Fluid Mechanics*, vol. 562, pp. 415–429, 2006.

[20] P. L. Brower, *Design of a manta ray inspired underwater propulsive mechanism for long range, low power operation [Master of Science]*, Tufts University in Mechanical Engineering, 2006.

[21] N. Kato, "Locomotion by mechanical pectoral fins," *Journal of Marine Science and Technology*, vol. 3, no. 3, pp. 113–121, 1998.

[22] N. Kato, B. W. Wicaksono, and Y. Suzuki, "Development of biology-inspired autonomous underwater vehicle 'Bass III' with high maneuverability," in *Proceedings of the International Symposium on Underwater Technology (UT '00)*, pp. 84–89, Tokyo, Japan, May 2000.

[23] K. H. Low, S. Prabu, J. Yang, S. W. Zhang, and Y. H. Zhang, "Design and initial testing of a single-motor-driven spatial pectoral fin mechanism," in *Proceedings of the IEEE International Conference on Mechatronics and Automation (ICMA '07)*, pp. 503–508, Harbin, China, August 2007.

[24] P. R. Bandyopadhyay, *Biomimetics Research at NUWC Video (Edited)*, 14 Mts, Naval Undersea Warfare Center, Newport, RI, USA, 2000.

[25] J. D. Geder, J. Palmisano, R. Ramamurti, W. C. Sandberg, and B. Ratna, "Fuzzy logic PID based control design and performance for a pectoral fin propelled unmanned underwater vehicle," in *Proceedings of the International Conference on Control, Automation and Systems (ICCAS '08)*, pp. 40–46, Seoul, Republic of Korea, October 2008.

[26] Y. R. Cai, S. S. Bi, and L. C. Zheng, "Design and experiments of a robotic fish imitating cow-nosed ray," *Journal of Bionic Engineering*, vol. 7, no. 2, pp. 120–126, 2010.

[27] C. L. Zhou and K. H. Low, "Better endurance and load capacity: an improved design of manta ray robot (RoMan-II)," *Journal of Bionic Engineering*, vol. 7, pp. S137–S144, 2010.

[28] S.-B. Yang, J. Qiu, and X.-Y. Han, "Kinematics modeling and experiments of pectoral oscillation propulsion robotic fish," *Journal of Bionic Engineering*, vol. 6, no. 2, pp. 174–179, 2009.

[29] R. Hu, W. B. Wang, Q. L. Guo, H. Wang, and F. Cao, "Design of bionic robofish with flapping-win," *Journal of Shihezi University*, vol. 28, no. 1, pp. 109–112, 2010.

[30] K. H. Low, "Modelling and parametric study of modular undulating fin rays for fish robots," *Mechanism and Machine Theory*, vol. 44, no. 3, pp. 615–632, 2009.

[31] A. Punning, M. Anton, M. Kruusmaa, and A. Aabloo, "A biologically inspired ray-like underwater robot with electroactive polymer pectoral fins," in *IEEE Mechatronics and Robotics (MechRob '04)*, vol. 2, pp. 241–245, Aachen, Germany, 2004.

[32] N. Kato, "Application of study on aqua bio-mechanisms to ocean engineering," *Kaiyo Kogaku Shinpojiumu*, vol. 16, pp. 131–138, 2001.

[33] K. Takagi, M. Yamamura, Z.-W. Luo et al., "Development of a rajiform swimming robot using ionic polymer artificial muscles," in *Proceedings of the IEEE/RSJ International Conference on Intelligent Robots and Systems (IROS '06)*, pp. 1861–1866, San Diego, Calif, USA, October 2006.

[34] J. Tangorra, P. Anquetil, T. Fofonoff, A. Chen, M. Del Zio, and I. Hunter, "The application of conducting polymers to a biorobotic fin propulsor," *Bioinspiration and Biomimetics*, vol. 2, no. 2, pp. S6–S17, 2007.

[35] Z. L. Wang, G. R. Hang, J. Li, Y. W. Wang, and K. Xiao, "A micro-robot fish with embedded SMA wire actuated flexible biomimetic fin," *Sensors and Actuators A: Physical*, vol. 144, no. 2, pp. 354–360, 2008.

[36] Y. Wang, Z. Wang, J. Li, and G. Hang, "Development of a biomimetic manta ray robot fish actuated by shape memory alloy," *Robot*, vol. 32, no. 2, pp. 256–261, 2010.

[37] K. H. Low and A. Willy, "Biomimetic motion planning of an undulating robotic fish fin," *Journal of Vibration and Control*, vol. 12, no. 12, pp. 1337–1359, 2006.

[38] W. M. Kier and J. T. Thompson, "Muscle arrangement, function and specialization in recent coleoids," in *Proceedings of the 1st International Symposium: Coleoid Cephalopods through Time*, Berlin, Germany, September 2002.

[39] Z. Chen, S. Shatara, and X. Tan, "Modeling of biomimetic robotic fish propelled by an ionic polymermetal composite caudal fin," *IEEE/ASME Transactions on Mechatronics*, vol. 15, no. 3, pp. 448–459, 2010.

[40] S. Guo, T. Fukuda, and K. Asaka, "A new type of fish-like underwater microrobot," *IEEE/ASME Transactions on Mechatronics*, vol. 8, no. 1, pp. 136–141, 2003.

[41] A. Azuma, *The Biokinetics of Flying and Swimming*, The American Institute of Aeronautics and Astronautics, Reston, Va, USA, 2nd edition, 2006.

[42] G. V. Lauder, E. J. Anderson, J. Tangorra, and P. G. A. Madden, "Fish biorobotics: kinematics and hydrodynamics of self-propulsion," *The Journal of Experimental Biology*, vol. 210, no. 16, pp. 2767–2780, 2007.

[43] K. H. Low, C. Zhou, and Y. Zhong, "Gait planning for steady swimming control of biomimetic fish robots," *Advanced Robotics*, vol. 23, no. 7-8, pp. 805–829, 2009.